Low Frequency Raman Active Vibrations in Fullerenes. 1. Monopolar Modes

Hans-Jürgen Eisler, Stefan Gilb, Frank H. Hennrich, and Manfred M. Kappes*

Institut für Physikalische Chemie, Universität Karlsruhe, 76128 Karlsruhe, Germany

Received: September 14, 1999

Raman measurements and PM3 calculations of low frequency (<600 cm^{-}) vibrational modes in a variety of different fullerenes can be rationalized in terms of the multipolar "acoustic" oscillations of isotropic spherical and spheroidal shells. In this first of a two part series, we show that all fullerene cages have monopolar-like breathing vibrations. Within certain boundary conditions and in the absence of other data, the frequency of these vibrations may be used for cage size determination.

Introduction

Since the first isolation of C_{60},[1] it has proven possible to generate, extract, and separate many other heavier members of the fullerene family (C_{2n}).[2] So far, all high fullerenes to be structually characterized have isolated pentagon ring structures (IPR forms).[3] On the basis of mathematical arguments, it can be shown that the smallest fullerene able to support an IPR form is C_{60}. C_{62}, C_{64}, C_{66}, and C_{68} do not have IPR isomers. Thereafter all C_{2n} have an IPR form. Starting at C_{76} multiple IPR isomers are possible. Within the IPR constraint, it has been argued that there are two isolable classes of fullerenes differing in their electronic structure:[4] (A) fullerenes with moderate to large HOMO−LUMO gaps and (B) those with small HOMO−LUMO gaps. The former class comprises practically all isolated and structurally characterized high fullerenes so far known. Its members are readily soluble in apolar solvents, are quite stable under ambient conditions and usually are among the energetically most favorable IPR isomers for a given cage size. It has recently been shown that class B fullerenes, such as C_{74}, are also generated in the Krätschmer−Huffman carbon arc source but that their enhanced reactivity (for which a marker may be high electron affinity[5]) relative to class A, generally precludes conventional extraction.[4] C_{72} is the only apparent exception to the two class picture: its calculated gap is large but it has not yet been isolated.[5]

Notable isolated members of class A include C_{60}, C_{70}, C_{76}, and C_{78} (three isolated isomers: C_{2v}, C_{2v}', and D_3), C_{80} (D_2)[2], C_{82} (mixture of two C_2 forms[6]), and C_{84} (2 isolated isomers: D_2 and D_{2d}[7]). For all of these not only the cage symmetry but also the molecular structure is known (a common complication for large C_{2n} is that several IPR isomers may have the same ^{13}C NMR signature in terms of the number of spectral lines and their relative peak intensities[8]). Beyond these cages it has proven possible to isolate multiple, size monodispersed and sometimes isomer pure fractions of even larger fullerenes by "conventional" chromatographic means.[9] So far the largest species to be so prepared is C_{120}.[6,10] Here, while the underlying cage symmetries are in fact unknown in the absence of enough isolated material to perform ^{13}C NMR measurements, the relatively simple solution absorption spectrum has been used to argue for the presence of just one or at worst a few isomers and the prevalence of cylindrical tubelet form(s) versus more spherical structure(s).

The inference that fullerene C_{120} has nanotubelet topology is also of interest from the point of view of single walled carbon nanotubes (SWNT). Recent advances in the SWNT field include diameter selective ablation syntheses[11] as well as the development of methods to cut and solubilize length and diameter controlled tubelets.[12] It may be anticipated that this approach will eventually yield soluble size selected tubelets which access the fullerene extraction size range. Given that there are already well developed chemical routes to link fullerene cages,[13] such size overlap will greatly facilitate the controlled synthesis of fullerene/SWNT supramolecular assemblies. For this, it will be necessary to characterize molecular topology of materials in the C_{100}−C_{300} range, for extremely small sample sizes.

^{13}C NMR measurements on nonisotope enriched samples require at least 10 mg of monodispersed material, even more if the sample comprises a wide distribution of different low symmetry isomers. Neutron and X-ray scattering probes at present technology typically make use of even larger samples. Given the rapidly decreasing abundance of class A fullerenes in arc discharge soot together with their decreasing solubility as n increases, it is unrealistic to expect to be able to prepare size and isomer pure samples containing more than about 10 μg of a given C_{2n}, $n > 50$, at least without heroic effort or a dramatic improvement in production yield. A similar restriction will undoubtedly apply to solubilized tubelets. How then to determine molecular structure or at least molecular topology for such extremely small samples? In this paper and its companion we present an approach which makes use of (resonant) Raman spectroscopy. We argue that the characteristic low-frequency vibrational features of closo-carbon networks, in particular monopolar and quadrupolar acoustic modes, facilitate a rapid cage size and topology determination by means of acquiring Raman spectra in the 50−600 cm^{-1} range.

The series is structured as follows. In the first paper we provide a general discussion of experimental and theoretical methods and concentrate on monopolar-like "breathing" modes. The second paper goes on to discuss quadrupolar-like "squashing" oscillations.

2. Methods

2.1. Materials. C_{60} (I_h) and C_{70} (D_{5h}) were obtained from commercial sources (Hoechst−Gold grade). Other fullerenes were prepared and extracted from raw soot as previously described.[2] Isomer pure samples of C_{70} (D_{5h}), C_{76} (D_2), C_{78} (C_{2v},

10.1021/jp9932665 CCC: $19.00
Published on Web 02/04/2000

C_{2v}', and D_3) and C_{80} (D_2)[2] were obtained by preparative scale HPLC using separation protocols which have also been previously described. C_{82} and C_{84} were obtained as isomer mixtures following separation on an Regis Buckyclutcher column (toluene/hexane eluent). We assume these mixtures to be comprised of C_{82} ($C_2(1)+C_2(2)$ (unknown ratio and C_{84} ($D_2(22)+D_{2d}(23)$/2:1), based on ^{13}C NMR measurements and comparison to literature.[6,7,15]

Microcrystalline fullerene samples for Raman spectroscopy were obtained from HPLC fractions in toluene solution as follows. The solutions were dried and the resulting solids ultrasonically dispersed in methanol. These suspensions were subsequently filtered (0.45 μm pore size). The solids so obtained were then washed multiply with methanol and dried under vacuum for 12 h. For each fullerene, sample purity was checked via analytical HPLC and LD-TOF-MS (laser desorption time-of-flight mass spectrometry) as previously described. Materials were studied at purity levels of > 99% relative to other cage sizes and at >95% relative to other isomers of the same cage size.

For Raman measurements two different sample preparation techniques were used, depending on relative cage stability. The more ambient stable fullerenes were studied as deposited on the microfilter (microcrystalline and optically thick films). The more sensitive higher fullerenes $C_{78}(C_{2v}')$, C_{80} (D_2), and C_{82} were sealed under vacuum ($<10^{-5}$ mbar) into a glass capillary and studied therein (microcrystalline powders).

2.2. Raman Measurements. Stokes shifted unpolarized Raman spectra, nominally at room temperature, were recorded in 180° backscattering geometry using four different laser excitation wavelengths. Measurements at 514, 693, and 794 nm were obtained using a triple monochromator setup (Spex TripleMate 1877D) and a CCD camera (Photometrics SDS 9000), as has been previously described.[14] Excitation radiation was provided by an Ar^+-pumped titanium sapphire laser (680−850 nm tunablility) as well as by the pump laser (514 nm). Spectra were recorded at typical laser fluences of 150−200 mW mm^{-2}. To reduce the broad-band luminescence of the titanium:sapphire laser we made use of a home-built premonochromator. Measurements at 794 nm were generally performed by replacing the first stage of the monochromator with an alkali vapor cell which allows for more efficient suppression of the Rayleigh line, while transmitting more Raman light. A number of Raman measurements were also performed using an FT-Raman spectrometer (Bruker IFS FRA 106) equipped with a Nd:YAG excitation laser (1064 nm, 140 mW defocused spot). Depending on effective scattering cross sections, spectra recorded at 514, 693, and 794 nm excitation were obtained at 2−4 cm^{-1} resolution using a 1200 line/mm grating. Raman data obtained at 1064 nm excitation were recorded with a spectral resolution of ~4 cm^{-1}.

Raman spectra were obtained for the isomerically pure fullerenes C_{60} (I_h), C_{70} (D_{5h}), C_{76} (D_2), C_{78} (C_{2v}, C_{2v}', D_3), C_{80} (D_2) as well as for C_{82} and C_{84} isomer mixtures (see above). With the exception of 1064 nm measurements for C_{60} and C_{70}, all spectra correspond to resonance or preresonance Raman conditions (see discussion below). Data were generally obtained in the Stokes shift range of approximately 100−1700 cm^{-1} at all four laser excitation wavelengths (exceptions C_{78} (C_{2v}, C_{2v}'), C_{80} (D_2), C_{82}, and C_{84}, for which background luminescence or other experimental difficulties prevented the acquisition of satisfactory spectra at 514 nm excitation). Figure 1 shows the corresponding spectra for 693 nm excitation. Raman features with S/N ratios >2−3 were fitted with Lorentzians in order to obtain peak positions and intensities.

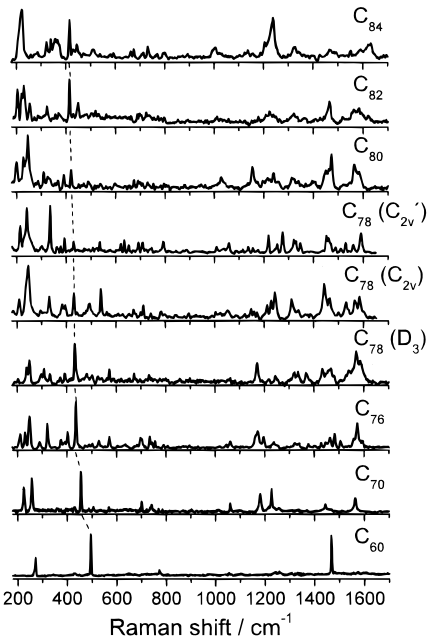

Figure 1. Stokes shifted unpolarized Raman spectra (overview) obtained at 693 nm laser excitation for the isomerically pure fullerenes C_{60} (I_h), C_{70} (D_{5h}), C_{76} (D_2), C_{78} (C_{2v}, C_{2v}', D_3), C_{80} (D_2). Also shown are similar data for isomer mixtures of C_{82} and C_{84} (see text for details).

3. PM3 Calculations

Semiempirical PM3 calculations of electronic ground states and vibrational frequencies were performed for all of the fullerenes probed experimentally. This was done using one of two computer systems (IBM Power PC (RISC 6000: AIX 4.21/128 MB RAM) or a PC (AMD processor 200 MHz/128 MB RAM) running the software package HyperChem (version 4.5)). The electronic ground-state structure of each fullerene was optimized beginning from well-established literature connectivities where available (C_{60} (I_h), C_{70} (D_{5h}), C_{76} (D_2), C_{78} (C_{2v}, C_{2v}', D_3), C_{80} (D_2), and C_{84} (D_2 (22), D_{2d} (23)[7,8]). In the case of C_{82} we have calculated all 9 possible IPR isomers and have come to the same conclusion as Zerbetto et al.[15] concerning their energetic ordering. On the basis of ref 15 we assume that the two lowest energy forms, no. 1 C_{82} (C_2) and no. 3 C_{82} (C_2), are present in our sample in unknown ratio.

Additionally we have performed PM3 calculations on a number of larger fullerene cages which are hypothetical at present in that they have not been isolated and/or structurally characterized. The focus in these calculations was to study the vibrational properties of cages with extreme topologies, i.e., either near-spherical or (cylindrical) tubelet. For these, the accessible fullerene size range was limited to about 140 atoms by the computing time required for vibrational frequency analysis. PM3 calculations were performed for C_{90} (D_{5h}, in terms of the SWNT nomenclature a (5,0) tubelet with the same diameter as C_{60}), C_{140} (D_{5d}, (5,0) tubelet) and C_{140} (I, near-spherical). The corresponding starting geometries were obtained in a two step procedure. First, the ring-spiral algorithm was used to obtain rough atomic coordinates.[16] This geometry was then refined using an extended Hückel algorithm prior to PM3 calculations.

Within the HyperChem software package we used the restricted Hartree−Fock method without configuration interac-

TABLE 1: Fullerene Cage Moments of Inertia[a]

fullerene/symmetry	I_a	I_b	I_c
C_{60}/I_h	10032	10032	10032
C_{70}/D_{5h}	12366	14374	14374
C_{76}/D_2	14398	16285	17880
C_{78}/D_3	14712	18264	18264
C_{78}/C_{2v}	15697	17331	17956
C_{78}/C_{2v}'	15168	17654	18273
C_{80}/D_2	15577	18638	19639
C_{82} (no. 1)/C_2	16727	19734	19984
C_{82} (no. 3)/C_2	17311	19038	19967
C_{84}/D_{2d}	19624	19660	19673
C_{84}/D_2	19095	19222	20729
C_{90}/D_{5d}	17093	26253	26261
C_{140}/I	54307	54408	54689
C_{140}/D_{5h}	28681	82562	82566

[a] In units of g cm^2 ($\times 10^{-40}$) based on optimized PM3 coordinates.

TABLE 2: Comparison of Scaled PM3 to Experimentally Determined Monopolar-Like Breathing Mode Frequencies

fullerene	unscaled PM3 frequency/cm^{-1}	experiment/ cm^{-1}	scaled PM3 frequency (factor 0.796)/cm^{-1}
C_{60}	623	496	496
C_{70}	571	455	455
C_{76}	542	436	431
C_{78} D_3	538	430	428
C_{78} C_{2v}	542	429	431
C_{78} C_{2v}'	536	434	427
C_{80}	528	421	420
C_{82} (no. 1) C_2	530		422
C_{82} (no. 3) C_2	529	420	421
C_{84} D_{2d}	524	415	417
C_{84} D_2	524	415	417

tion (RHF) to obtain ground-state structures. Energy minimization was driven by the Polack−Ribiere conjugate−gradient algorithm. In all cases self-consistence was achieved and the optimization terminated at root-mean square (rms) gradient of <0.01 kcal mol^{-1} Å^{-1}. Vibrational frequencies were calculated in the harmonic approximation for each ground-state structure. Table 2 of this paper and Table 1 of the following paper contain the calculated positions of monopolar and quadrupolar derived vibrations (see below).

4. Results and Discussion

4.1. Low-Frequency Acoustic Modes in C_{60}. *4.1.1. Lamb Theory*. It was first pointed out by Ceulemans et al.[17] that the low-frequency vibrations (<600 cm^{-1}), of near spherical C_{60}, may be quite well described in terms of the continuum mechanics of a vibrating hollow sphere. The eigenfunctions and eigenfrequencies describing the fundamental vibrations of both the isotropic (filled) elastic sphere[18] as well as the spherical shell (infinitely thin)[19] were first derived by Lamb more than a century ago. Lambs oscillatory solutions for the filled elastic sphere have been extensively applied to describing the particle size dependence observed for low frequency (Raman allowed) monopolar breathing vibrations in near-spherical nanocrystallites of various kinds.[20] Time-dependent coupling of electronic excitations to this kind of vibration is also of present interest.[21,22] The application of "Lamb theory" to hollow nanoparticles (=fullerenes) is not as extensive and a few words of explanation are in order.

Under the assumption that there are no "flexural" contributions to the potential energy (i.e., contributions due to twisting in the surface plane), Lamb finds two classes of solutions one involving purely tangential (I) and one involving both tangential and radial motion (II). Both classes of solution have eigenfunctions which transform as the spherical harmonics and are generally classified in terms of a descriptor l (= 0, 1, ...). For class I there is only one solution per l value, whereas class II has two solutions (a and b) per l, except for l(II) = 0 which has only one solution. The corresponding eigenvalues depend on the sphere radius, its first (="rigidity") and second Lamé elasticity constants, the Poisson ratio, and the volume density. The Poisson ratio may be related to the Lamé elasticity constants which in turn depend on the volume density as well as the transverse (c_t) and longitudinal (c_l) sound velocities in the isotropic shell material.[23] Class I solutions become real and nonzero for $l \geq 1$, whereas for class II there are nonzero solutions from $l = 0$ on up. From symmetry arguments and for allowed Poisson ratios (which can vary between 0 and 0.5), it can be shown that the lowest frequency Raman active solutions correspond to class II $l = 2$ (a) and $l = 0$ in order of increasing frequency. According to the usual nomenclature convention for spherical harmonics we label these D_g and S_g, respectively. In addition to schematic representations of the corresponding oscillatory motions (→ eigenfunctions) for these two Raman active quadrupolar and monopolar vibrations, Figure 2 contains a plot of all class I and II eigenvalues below 1500 cm^{-1} using as input the radius of C_{60} (0.35 nm[24]) as well as experimental values for the longitudinal (21 km s^{-1}) and transverse (12.3 km s^{-1}) sound velocities of three-dimensional graphite.[25]

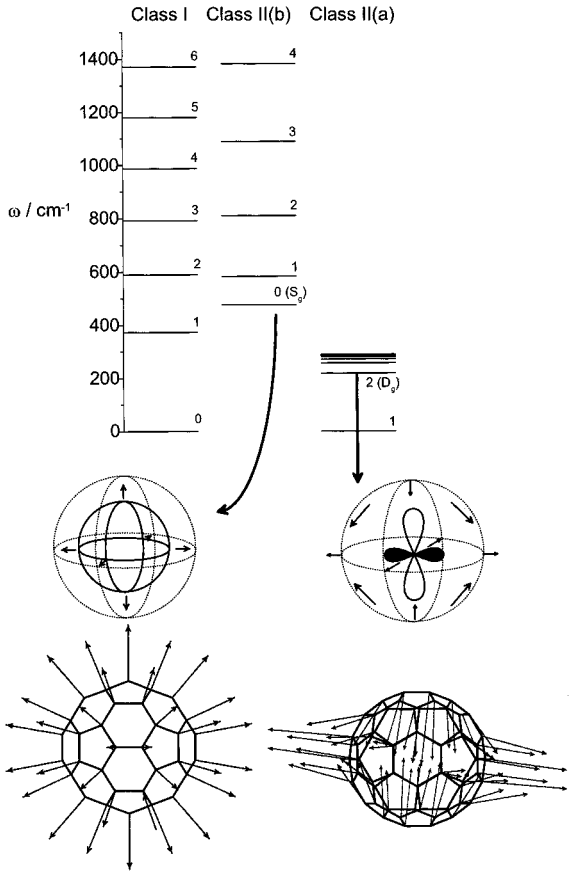

Figure 2. Level diagram of Lamb theory oscillatory solutions for a C_{60}-like isotropic spherical shell (see text). Also shown are visualizations of the (lowest energy) Raman active D_g and S_g solutions in comparison to PM3 derived representations of the corresponding Raman allowed $H_g(1)$ and $A_g(1)$ modes.

We concentrate in the following on the $l = 0$ solution and return to the $l = 2$ solution in the next paper of the series. The corresponding vibrational motion is that of a fully symmetric

radial breathing mode. From Lamb[19] the angular frequency of this monopolar mode is given in terms of the longitudinal and transverse sound velocities by eq 1:

$$\omega = 2(c_t^2(3c_l^2 - 4c_t^2)/c_l^2)^{1/2}/R \quad (1)$$

Note first that this equation predicts that the corresponding vibration should scale as $1/R$. We will return to this point below. Note further, that if we insert into eq 1 the measured sound velocities of 3-D graphite and the radius of C_{60} we obtain a remarkably good prediction of the monopolar mode vibrational frequency of 476 cm^{-1} compared to the experimental determination from the Raman spectrum obtained for the molecular solid at room temperature, which lies at 496 cm^{-1}. The reason that a classical model parametrized to the bulk does quite well at describing a low frequency "acoustic" vibration in this molecule appears to be 2-fold. First, the distance sound travels in graphite during the breathing mode period is comparable to the circumference of the fullerene cage ($c_l\tau_{l(II)=0} = 1.5$ vs 2.2 nm; i.e., the detailed atomic position is of secondary importance) and second the vibrational properties of C_{60}, in particular the average C−C stretching force constant, must be analogous to planar graphene. We discuss this point in more detail below.

4.1.2. Stretching Force Constant Model. To obtain insight into the magnitude of the C−C stretching force constant in C_{60} it is useful to consider a one parameter pseudo molecular model of the fully symmetric vibration.

For clarity we begin with a simpler molecular system comprising a carbon ring. For our purposes we define as a ring a molecule with *N*-atoms lying on the vertexes of a regular N-polygon with polygon center-to-atom distance *R*. In a totally symmetric breathing vibration of such a species, all atoms move radially out from the center with the same phase and amplitude. There are no changes to relative bond angles, consequently we can attempt to describe the vibration purely in terms of a uniform stretching force constant. Principle geometric considerations show that for a radial displacement from equilibrium d*R*, the component springs connecting two adjacent atoms are extended by $da = 2(a/R)\ dR^2$, where *a* is the C−C bond distance. Consequently the potential energy for the *N* atoms (and therefore *N* springs) ring becomes $V = 2Nf(a^2/R^2)\ dR^2$, where *f* is the stretching force constant. Similarly the total kinetic energy for the ring as it undergoes a breathing vibration is given by $T = Nmd\dot{R}^2$ where $d\dot{R}$ corresponds to $d(dR)/dt$. Then, using the Lagrange equation of motion $(d/dt(\delta T/\delta(d\dot{R})) + \delta V/\delta R = 0)$, inserting the expressions for *T* and *V* and the general solution $dR = R_0e^{i\omega t}$ we obtain eq 2 which provides a relationship between the ring breathing mode angular frequency and the atomic mass, stretching force constant, interatomic separation, and radius.

$$\omega_{ring} = a\,(f/m)^{1/2}/R \quad (2)$$

For the fully symmetric breathing mode of a "spherical" fullerene the approach is analogous. However, in contrast to rings, it is important to remember that there is no generally valid way of positioning *N*-objects uniformly on the surface of a sphere. Nevertheless for computational simplicity, we assume that the consequences of this topological problem become negligible for large *N*. Specifically we connect each atom to its three neighbors with the same spring (force constant *f*) and the same equilibrium interatomic separation a. For an Euler polyhedron with (12) pentagons and hexagons there are 3*N*/2 springs (=edges). Again for a radial displacement from equilibrium d*R*, the increase in potential energy is of the form $V = 3Nf\,(a^2/R^2)dR^2$. At the same time, the kinetic energy of all atoms moving in phase either away or toward the sphere center is given by: $T = Nmd\dot{R}^2$. Inserting into the Lagrangian as for the ring, we obtain eq 3, which connects the spherical fullerene monopolar breathing mode to the force constant, interatomic separation, atomic mass, and sphere radius.

$$\omega_{fullerene} = (3f/2m)^{1/2}\ a/R \quad (3)$$

Both eqs 2 and 3 have an $1/R$ dependence. Interestingly, if the same force constant and interatomic separation is used in both formulas, the one parameter spring model predicts that the slope of ω vs $1/R$ should be exactly $(^3/_2)^{1/2}$ times larger for spherical cages than for rings.

The analytic formula obtained for spherical fullerenes may be used to assess the underlying force constant by comparison to C_{60}. If we insert the particle radius (350pm), the experimental breathing mode frequency and an average C−C bond length of 142.9 pm, we obtain an effective C−C stretching force constant of 7 aJ $Å^{-2}$. This compares with tabulated values of 4.50, 9.6, 15.59 aJ $Å^{-2}$ for carbon−carbon single, double, and triple bonds.[26] Note that the corresponding value for 3-D graphite (obtained from the elastic constants of graphite) is 7.1 aJ $Å^{-2}$.[27]

4.1.3. Normal Coordinates from PM3. PM3 semiempirical quantum chemical calculations have generally been found to be in good qualitative agreement with experiment for a variety of fullerene related solids.[14] Apart from ground state structures and energetics, PM3 routinely provides vibrational frequencies and the corresponding normal coordinates. Figure 1 also contains a PM3 visualization of the two lowest frequency Raman allowed modes in C_{60} ($H_g(1)$ and $A_g(1)$). It is apparent that the vibrational motion corresponds very closely to the Lamb theory expectation for quadrupolar and monopolar oscillations in isotropic spherical shells.

For fullerenes and related molecules, PM3 derived vibrational frequencies are generally predicted to lie somewhat higher than observed in experiment. For C_{60} and C_{70}, there are detailed spectral assignments, which can be used to gauge the exact PM3 scaling factors required to quantitatively describe experiment.[28] Unfortunately, the theory is not uniformly off. Corrections to PM3 prediction in fact depend on the frequency range and vibration type in question (ranging from 0.76 to 1.01 for C_{60}, with an average of 0.883). For C_{60} and C_{70} breathing modes which are of interest here one obtains a scaling factor of 0.796 and 0.797, respectively. We use the average (0.796) as the "PM3 scaling factor" in the remainder of this paper.

4.2. Monopolar-Like Vibrations in High Fullerenes? *4.2.1. Scaled PM3 Calculations*. To what extent can (larger) cages of lower symmetry than C_{60} (I_h) sustain monopolar-like vibrational modes, i.e., vibrations which are characterized by the presence of a nodal surface coinciding essentially with the equilibrium cage? Inspection of visualized normal modes derived from PM3 calculations for all experimentally accessed cages, indicates that there is always one such totally symmetric Raman allowed vibration at low frequency. There are no other similar vibrations. Figure 3 provides images of the corresponding "monopolar-like" vibrational motions.

To investigate whether this is in fact a general feature of fullerenes we next consider PM3 calculations for hypothetical fullerenes C_{90} (D_{5h}) and C_{140} (D_{5d} and I). All three molecules also show a single monopolar-like vibration as evidenced in Figure 3. Note, however, that the vector magnitudes and orientations describing the breathing mode motion of the atoms in tubelet and near-spherical C_{140} are subtly different. In the

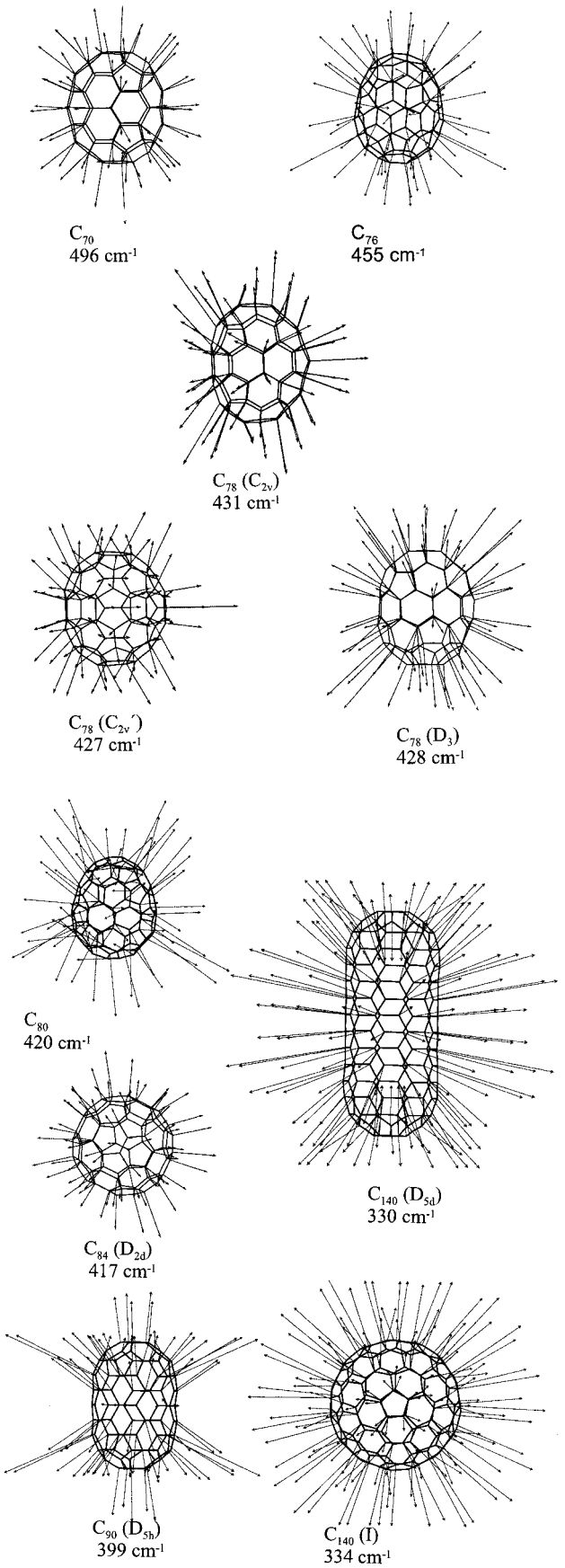

Figure 3. Visualizations of monopolar-like "breathing-modes" in several high fullerenes as determined from PM3 calculations. Also shown are scaled frequencies. Note that the cage size is not to scale.

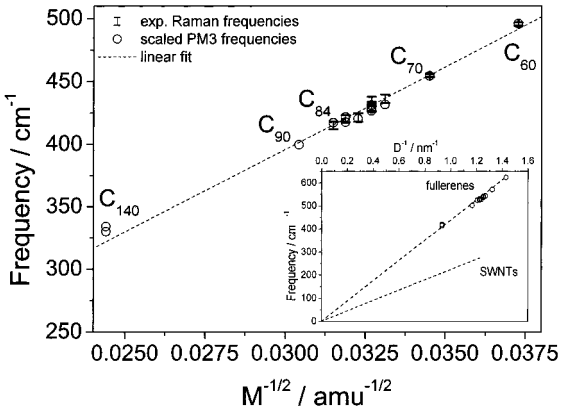

Figure 4. Scaled PM3 "breathing-mode" frequencies vs $M^{-1/2}$ where M is the fullerene molar mass. Superimposed are experimental determinations based on spectral assignment as discussed in the text. The dashed line is a least-squares fit to the scaled breathing mode frequencies for all fullerenes calculated, constrained to go through the coordinate origin. The insert documents the full x-axis parameter range. Here instead of using $M^{-1/2}$ we plot $1/D$ where D corresponds to the diameter of a spherical fullerene with the same surface area A (A is proportional to M). The second dashed line in the insert represents the diameter dependence of the radial breathing mode of single walled carbon nanotubes (SWNTs).

more cylindrical isomer, the end-cap motion appears out of phase with the periodic expansion/contraction of the tubelet cross section. In fact already for tubular C_{90}, the concept of a "single nodal-surface monopolar-mode" is not strictly accurate in that the end caps are partially drawn in while the rest of the molecule expands.

Figure 4 contains a plot of scaled PM3 breathing mode frequencies versus $M^{-1/2}$ for all C_{2n} fullerene cages studied, where M corresponds to the fullerene molar mass ($2\ nmN_{Av} = M$; N_{Av} = Avogadro number). Interestingly, the data points (even those for $C_{90}(D_{5h})$ and $C_{140}(D_{5d})$) generally fall very close to a least-squares fit line with a slope of 13195 cm^{-1} $amu^{1/2}$, constrained to go through the coordinate origin. This manifests a correlation coefficient of $R^2 = 0.9911$. We then infer that (i) the frequency of monopolar-like modes goes approximately as $M^{-1/2}$ and (ii) for multiple isomers of a given cage size, the frequency of the monopolar-like mode does not depend strongly on shape. Among structurally characterized fullerenes, several are known to be more spherical than others. This may be quantified in terms of their moments of inertia, which are tabulated in Table 1. Of those cages studied here, the most spherical are C_{60}, $C_{84}(D_2)$ (to a lesser extent $C_{84}(D_{2d})$) and C_{140}-(I). On the basis of the $1/R$ dependency predicted for *spherical* shells in 4.1.1 and 4.1.2 (assuming that sound velocities/average stretching force constants are not strongly cage size dependent), one might expect scaled PM3 breathing mode frequencies for more spherical cages to be in better agreement with an $M^{-1/2}$ dependence than the complete data set. This is not obviously the case (least-squares fits: (i) $\omega_1(S_g) = 349$ [cm^{-1} nm]/$\langle D\rangle$ and $R^2 = 0.9979$ for just the spherical fullerenes with coordinate origin constraint, (ii) $\omega_1(S_g) = 344$ [cm^{-1} nm]/$\langle D\rangle$ and $R^2 = 0.9911$ for all fullerenes also with coordinate origin constraint, where $\langle D\rangle$ corresponds to the diameter of a spherical fullerene in nanometers).

4.2.2. Comparison to Experiment. Using the average of the PM3 ↔ experiment scaling factors found for the breathing modes of C_{60} and C_{70}, PM3 predictions for the monopolar-like modes of high fullerenes are expected to be quite accurate. Unfortunately, PM3 does not allow the determination of the associated Raman cross sections (in particular of resonant Raman cross sections which are generally probed here). Therefore comparison to experiment which typically shows a

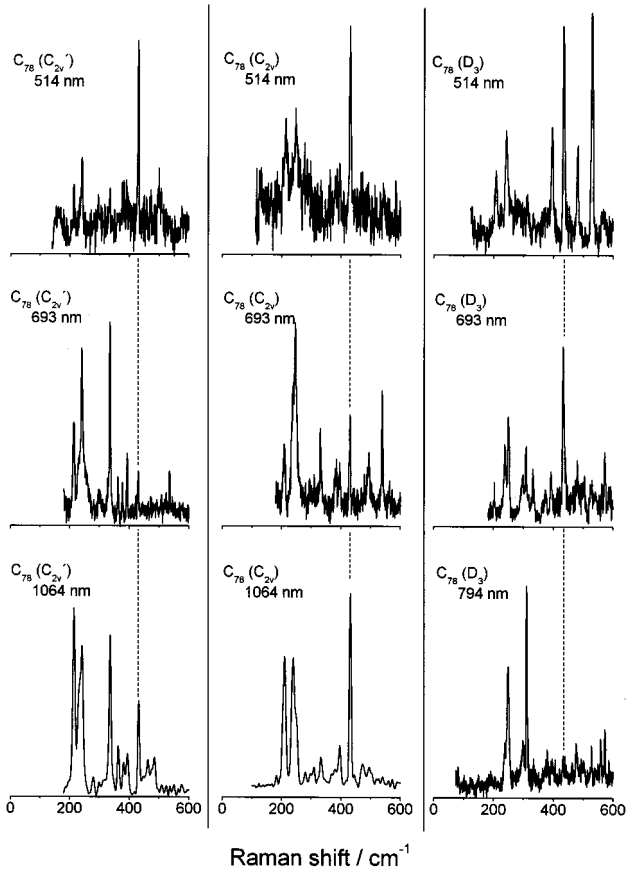

Figure 5. Low-frequency region Raman spectra obtained for three C_{78} isomers at several different laser excitation wavelengths. Superimposed are scaled PM3 frequencies for Raman allowed vibrations. Assigned breathing modes are indicated with dashed lines (see also Table 1).

high density of vibrational features in the relevant spectral region is problematic.

Nevertheless, breathing modes may generally be assigned by comparing spectra obtained at several different excitation wavelengths. Figure 5 shows as an typical example the spectra obtained for the three isomers of C_{78}, at 514, 693, and 1064 nm (794 nm in the case of the D_3 isomer) excitation. Superimposed are PM3 predictions scaled to C_{60}/C_{70} experiment. Within the range predicted for the breathing mode, there is generally only one Raman spectral feature which manifests moderate to strong Raman cross section over all excitation wavelengths probed. This we assign as the breathing mode. For all other fullerenes experimentally probed here, the experiment/theory comparison is as good or better than shown for the C_{78} isomers. Table 2 lists scaled PM3 breathing mode frequencies and experimental assignments. In future work, it will be of interest to confirm this assignment by comparing to resonant Raman cross sections calculated at an ab initio level of theory. The associated electronically excited states have already been assigned on the basis of predictive level time-dependent-density functional calculations.[29]

4.2.3. Monopolar Modes and Spheroidal Distortions. We return briefly to a discussion of the shape insensitivity observed for the monopolar mode frequencies of cage isomers. As an example, the three isomers of C_{78} manifest breathing modes at 429, 434, and 430 cm^{-1} for C_{2v}, C_{2v}' and D_3 isomers, despite a relatively large variation in topology. Even more pronounced is the shape variation between C_{140} (D_{5d}) and C_{140} (I) while the associated monopolar modes at 414 and 420 cm^{-1} are predicted to be almost identical in frequency. Interestingly, a

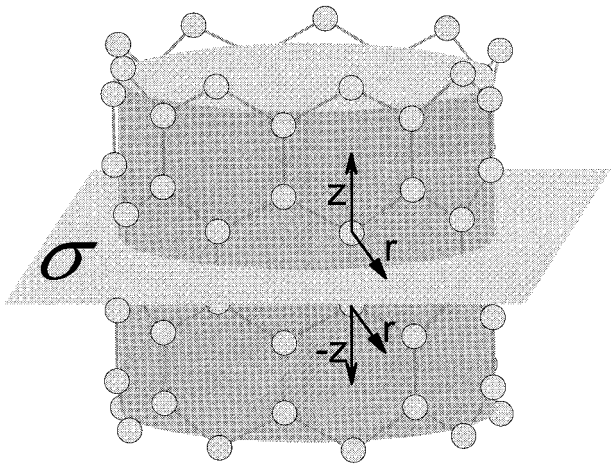

Figure 6. Schematic of radial breathing mode in single-walled carbon nanotubes.

first-order perturbation theory treatment applied to the Lamb oscillatory solutions for *filled* spheres subject to small spheroidal distortion predicts that the $l = 0$ modes should not shift as long as volume is conserved in the distortion. This is in contrast to oscillatory solutions of higher l for which a distortion dependent splitting is predicted (we shall return to the latter in the context of quadrupolar modes in the next paper). To our knowledge, such a first-order perturbation theoretical treatment has not yet been applied to the spherical shell subject to spheroidal distortion. On the basis of our observations we would expect the resulting expression to be of a form such that the monopolar mode remains invariant for spheroidal distortions *conserving surface area*. It will be interesting to see if this prediction is born out in future theoretical treatments.

4.3. Radial Breathing Modes in Single Walled Carbon Nanotubes. Near infinite length single walled carbon nanotubes (SWNT) are known to manifest a Raman active radial breathing mode whose frequency scales inversely with the tube radius, independent of whether the specific tube is metallic, semiconducting or insulating. This vibration is in fact already used as a diagnostic for tube diameter (D) distribution.[30−32] Parametrization against high resolution electron microscopic images allows determination of the exact scaling factor. One finds that the radial breathing mode depends inversely on diameter according to 223 cm^{-1} nm/D.[33] We have plotted this $1/D$ dependence as a dashed line in the insert of Figure 3. The insert also contains the analogous representation for fullerenes − taking D for a given fullerene C_{2n} as the diameter of a spherical cage with the same number of atoms $2n$. Note that atom count/molar mass scale as surface area and therefore $M^{-1/2} \alpha 1/D$.

The slope of the fullerene line is almost exactly 1.5 times larger than that describing the $1/D$ dependence of SWNT radial breathing vibrations. Is this a straightforward consequence of dimensionality/topology much as the $(^3/_2)^{1/2}$ ratio discussed in 4.1.2 for the breathing modes of rings and spheres?

Applying the simple force constant model to SWNTs shows that the answer is no. We demonstrate this below for infinitely long zigzag tubes; however, similar considerations lead to the same results for armchair tubes. Like a graphene sheet, SWNTs have two symmetry inequivalent atoms connected by three symmetry inequivalent bonds. It is convenient to use cylindrical coordinates to describe the vibrational motion of the tube: r describes the radial displacement, z the displacement parallel to the tube axis, and t the displacement perpendicular to both. So in principle six coordinates are needed to describe the periodic displacements of the two inequivalent atoms in a totally

symmetric breathing mode. Fortunately, this number can be reduced to two. Reflection through a mirror-plane perpendicular to the *z*-axis transforms one symmetry inequivalent atom to the other (see Figure 6). As a consequence, in a radial breathing vibration all atoms undergo the same motion with regard to *r*,*t* while symmetry inequivalent atoms move in opposite directions with regard to *z* (if both types of atom were to undergo the same motion with respect to *z* a translation would ensue). The same *t* motion of all atoms in a zigzag tube means a rotation. This is incompatible with a vibration ($\rightarrow t = 0$) and therefore only two coordinates (*r*,*z*) are sufficient to describe the totally symmetric radial breathing vibration of a SWNT.

A closer look at the displacement of this vibration shows that not only bond length changes but also a change in the C−C−C angle occurs. So in contrast to our discussion for fullerenes, the potential energy of the SWNT model must now comprise two terms (for bond stretching and bending), dependent on two force constants (f_s and f_b/a^2) and two coordinates.

$$V_{\text{stretching}} = \frac{Nf_s}{2}\left[2z^2 + \left(\frac{3ar}{4R} - z\right)^2\right] \tag{4}$$

$$V_{\text{bending}} = \frac{Nf_b a^2}{4}\left[\left(\frac{2\sqrt{3}z}{a} - \frac{\sqrt{3}r}{2R}\right)^2 + 2\left(\frac{2\sqrt{3}z}{a} + \frac{\sqrt{3}r}{2R}\right)^2\right] \tag{5}$$

Putting this into the Lagrangian one gets two totally symmetric modes, after solving the two coupled differential equations. The one with the lower frequency is the breathing mode with mainly r-motion. The second one has mainly *z*-motion and a higher frequency. The relatively complicated expressions for the corresponding frequencies may be formulated in terms of a Taylor series expansion in *a*/*R*. Equation 6 gives the breathing mode frequency to first order in *a*/*R*.

$$\omega = \frac{\sqrt{3}}{4}\sqrt{\frac{2f_s^2 + 21f_sf_b + 18f_b^2}{(f_s + 6f_b)m}}\,\frac{a}{R} \tag{6}$$

We conclude that the breathing mode frequency depends on two parameters. Inserting into equation the C−C stretching force constant obtained from the spring model for fullerenes 7 aJ/Å^2, we have to use 1.7 aJ/Å^2 for the C−C−C bending force constant in order to obtain a slope of 223 cm^{-1} nm/D_{SWNT}. Setting the bending force constant to 0 aJ//Å^2, $f_s = 11.6$ aJ/Å^2 is needed to describe the slope of 223 cm^{-1} nm/D_{SWNT}. From the elastic constants (equivalent to the Lamé factors) of graphite one can obtain the values 7.1 aJ/Å^2 for the stretching and 0.67 aJ/Å^2 for the bending force constant.[27]

5. Conclusions

High fullerenes are shown to have Raman active monopolar-like breathing modes, much like the $A_g(1)$ mode of C_{60}. For fullerenes ranging in size at least to C_{140}, the frequency of the monopolar-like mode scales inversely with the square root of mass. For fullerene isomers of the same mass (and "surface area"), the monopolar mode frequency is shape insensitive. The breathing mode frequency and its size dependence can be rationalized both in terms of the oscillatory S_g mode of an isotropic spherical shell as well as in terms of an atomistic model incorporating, 3-fold connectivity, a single C−C stretching force constant and one average bond length. Near-infinite length single-walled carbon nanotubes have analogous radial breathing modes which however require the inclusion of flexural-motion for their quantitative description.

Acknowledgment. This research was supported by the Deutsche Forschungsgemeinschaft under SFB 551 "Kohlenstoff aus der Gasphase: Elementarreaktionen, Strukturen und Werkstoffe."

References and Notes

(1) Krätschmer, W.; Fostiropoulos, K.; Huffman, D. *Nature* **1991**, *347*, 354.
(2) Hennrich, F. H.; Michel, R.; Fischer, A.; Richard-Schneider, S.; Gilb, S.; Kappes, M. M.; Fuchs, D.; Bürk, M.; Kobayashi, K.; Nagase, S.; *Angewandte Chemie* **1996**, *108*, 1839; Hennrich, F. H.; Eisler, H.-J.; Gilb, S.; Gerhardt, P.; Wellmann, R.; Schulz, R.; Kappes, M. M. *Ber. Bunsen-Ges. Phys. Chem.* **1997**, *101*, 1605.
(3) Fowler, P.; Manolopoulos, D. *An Atlas of Fullerenes*; Clarendon Press: Oxford, 1995.
(4) Diener, M. D.; Alford, J. M. *Nature* **1998**, *393*, 668.
(5) Boltalina, O.; Dashkova, E.; Sidorov, L. *Chem. Phys. Lett.* **1996**, *256*, 253.
(6) Achiba, Y.; Kikuchi, K.; Aihara, Y.; Wakabayashi, T.; Miyake, Y.; Kainosho, M. *Mater. Res. Soc. Symp. Proc.* **1995**, *359*, 3.
(7) Dennis, T. J. S.; Kai, T.; Tomiyama, T.; Shinohara, H. *Chem. Commun.* **1998**, *1998*, 619.
(8) Schneider, U.; Richard, S.; Kappes, M. M.; Ahlrichs, R. *Chem. Phys. Lett.* **1993**, *210*, 165.
(9) Achiba, Y.; Kikuchi, K.; Aihara, Y.; Wakabayashi, T.; Miyake, Y.; Kainosho, M. *The Chemical Physics of Fullerenes 10 (and 5) Years Later*; Andreoni, W. Ed.; 1996; p 139.
(10) Iwasaki, K.; Umishita, K.; Hino, S.; Miyamae, T.; Kikuchi, K.; Achiba, Y. *Phys. Rev. B.* **1999**, *60*, 5044.
(11) Bandow, S.; Asaka, S.; Saito, Y.; Rao, A.; Grigorian, L.; Richter, E.; Eklund, P. *Phys. Rev. Lett.* **1998**, *80*, 3779.
(12) Chen, J.; Hamon, M.; Hu, H.; Chen, Y.; Rao, A.; A. Eklund, P.; Haddon, R. *Science* **1998**, *282*, 95.
(13) Lebedkin, S.; Ballenweg, S.; Gross, J.; Taylor, R.; Krätschmer, W. *Tetrahedron Lett.* **1995**, *36*, 4971. Gromov, A.; Lebedkin, S.; Hull, W.; Krätschmer, W. *J. Phys. Chem. A* **1998**, *26*, 4997.
(14) Eisler, H.-J.; Hennrich, F. H.; Werner, E.; Hertwig, A.; Stoermer, C.; Kappes, M. M. *J. Phys. Chem. A* **1998**, *102*, 3889.
(15) Orlandi, G.; Zerbetto, F. *J. Phys. Chem.* **1993**, *97*, 13575.
(16) Manolopoulos, D. E.; May, J. C.; Down, S. E. *Chem. Phys. Lett.* **1991**, *181*, 105.
(17) Ceulemans, A.; Fowler, P.; Vos, I. *J. Chem. Phys.* **1994**, *100*, 5491. Ceulemans, A.; Vos, I. *Mol. Phys.* **1991**, *72*, 1051.
(18) Lamb, H. *Proc. London Math. Soc.* **1882**, *13*, 189.
(19) Lamb, H. *Proc. London Math. Soc.* **1882**, *14*, 50.
(20) Saviot, L.; Champagnon, B.; Duval, E.; Ekimov, A. *Phys. Rev. B* **1998**, *57*, 341.
(21) For example of semiconductor nanocrystals, see: Cerullo, G.; De Silvestri, S.; Banin, U. *Phys. Rev. B* **1999**, *60*, 1928.
(22) For example metal nanoparticles, see: Del Fatti, N.; Voisin, C.; Chevy, F.; Vallee, F.; Flytzanis, C. *J. Chem. Phys.* **1999**, *110*, 11484.
(23) Landau, L.; Lifshitz, E. *Course of Theoretical Physics, 3rd ed.; Theory of Elasticity*; Pergamon Press: Oxford, 1998; Vol. 7.
(24) Liu, S.; Lu, Y.-J.; Kappes, M. M.; Ibers, J. A. *Science* **1991**, *254*, 408.
(25) Dresselhaus, M.; Dresselhaus, G.; Sugihara, K.; Spain, I.; Goldberg, H. *Graphite Fibers and Filaments*; Springer Series in Materials Science 5; Springer-Verlag: Berlin, 1988.
(26) Hollas, J. *High-Resolution Spectroscopy*; John Wiley & Sons: New York **1998**.
(27) See: Tuinstra, F.; Koenig, J. L. *J. Chem. Phys.* **1970**, *33*, 1126 and references therein.
(28) Brockner, W.; Menzel, F. *J. Mol. Struct.***1996**, *378*, 147.
(29) Bauernschmitt, R.; Ahlrichs, R.; Hennrich, F. H.; Kappes, M. M. *J. Am. Chem. Soc.* **1998**, *120*, 5052.
(30) Saito, R.; Takeya, T.; Kimura, T.; Dresselhaus, G.; Dresselhaus, M. *Phys. Rev. B* **1999**, *59*, 2388.
(31) For example, see: Kasaya, A.; Sugano, M.; Maeda, T.; Saito, Y.; Tohji, K.; Takahashi, H.; Sasaki, Y.; Fukushima, M.; Nishina, Y.; C. Horie, C. *Phys. Rev. B* **1998**, *57*, 4999.
(32) Kataura, H.; Kumazawa, Y.; Maniwa, Y.; Umezu, I.; Suzuki, S.; Ohtsuka, Y. Achiba, Y. *Synth. Met.* **1998**, *103*, 2555.
(33) Rao, A. M.; Bandow, S.; Richter, E.; Eklund, P. C. *Thin Solid Films* **1998**, *331*, 141.